ACS APPLIED MATERIALS & INTERFACES

Research Article

www.acsami.org

Charging System Optimization of Triboelectric Nanogenerator for Water Wave Energy Harvesting and Storage

Yanyan Yao,[†,§] Tao Jiang,[†,§] Limin Zhang,[†] Xiangyu Chen,[†] Zhenliang Gao,[†] and Zhong Lin Wang*[,†,‡]

[†]Beijing Institute of Nanoenergy and Nanosystems, Chinese Academy of Sciences, National Center for Nanoscience and Technology (NCNST), Beijing 100083, China

[‡]School of Materials Science and Engineering, Georgia Institute of Technology, Atlanta, Georgia 30332-0245, United States

Supporting Information

ABSTRACT: Ocean waves are one of the most promising renewable energy sources for large-scope applications due to the abundant water resources on the earth. Triboelectric nanogenerator (TENG) technology could provide a new strategy for water wave energy harvesting. In this work, we investigated the charging characteristics of utilizing a wavy-structured TENG to charge a capacitor under direct water wave impact and under enclosed ball collision, by combination of theoretical calculations and experimental studies. The analytical equations of the charging characteristics were theoretically derived for the two cases, and they were calculated for various load capacitances, cycle numbers, and structural parameters such as compression deformation depth and ball size or mass. Under the direct water wave impact, the stored energy and maximum energy storage efficiency were found to be controlled by deformation depth, while the stored energy and maximum efficiency can be optimized by the ball size under the enclosed ball collision. Finally, the theoretical results were well verified by the experimental tests. The present work could provide strategies for improving the charging performance of TENGs toward effective water wave energy harvesting and storage.

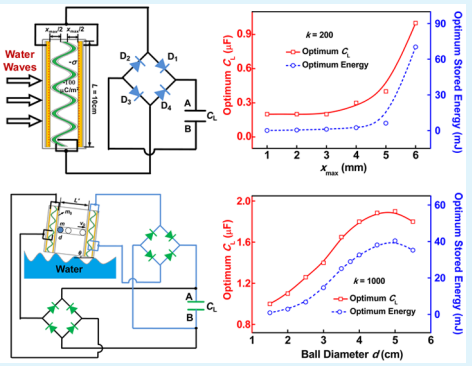

KEYWORDS: *triboelectric nanogenerator, water wave energy, charging characteristic, charging system optimization, energy storage efficiency, blue energy harvesting*

1. INTRODUCTION

With the growing threat of energy crisis and environmental deterioration, seeking new energy sources as substitutes for the traditional ones, such as ocean wave, wind, and solar energies, is of great importance in human production and living.[1−3] Among all of the new energy sources, ocean wave energy is superior because it is easily available, sustainable, and independent of season, climate, and weather conditions.[4,5] Previous converters for water wave motions were mainly based on electromagnetic generators by use of magnets, metal coils, absorber, and turbine, which are heavy, bulky, and inefficient at ocean wave frequency.[6−8] Therefore, it is greatly desirable to search for a lightweight, small-sized, cost-effective, and facile technology to convert water wave energy into electricity.

Recently, triboelectric nanogenerator (TENG) based on contact electrification and electrostatic induction has been invented as a promising technology for harvesting mechanical energy, which exhibits the advantages of high output power, high energy conversion efficiency, low weight, and fabrication cost.[9−13] It has been proved to have the ability to harvest water wave energy and be of huge potential toward large-scale blue energy harvesting from the ocean.[14−23] In our previous works, a TENG network design was proposed,[14,15] and a basic unit of the network was structurally optimized to reach the highest output performance.[16] From the theoretical and experimental results, it could be found that there exists an optimum ball size or mass to reach maximized output power and electric energy in a box-like device composed of wavy-structured TENG walls and an enclosed ball. Because of the uncontrollable and unstable nature of environmental water waves, the converted electrical energy from TENGs is unstable and cannot be directly used to power electronic devices. Therefore, an energy storage unit such as capacitor or battery is required to store the harvested energy and provide a regulated and manageable output.[24,25] However, until now the integration behavior of TENG with an energy storage unit is still unclear. In addition, the influence of structural parameters on charging characteristics of TENG and the issue about how to optimize its charging performance remain to be studied, which is critical for efficient water wave energy harvesting and storage.

In the present work, we discussed the characteristics of utilizing a wavy-structured TENG to charge a capacitor in two cases, that is, under the direct water wave impact and enclosed ball collision. On the basis of the theoretical model of wavy-structured TENG, the charging characteristics of TENG when imposed as a periodic triggering at a low frequency were

Received: June 24, 2016
Accepted: August 5, 2016

DOI: 10.1021/acsami.6b07697
ACS Appl. Mater. Interfaces XXXX, XXX, XXX−XXX

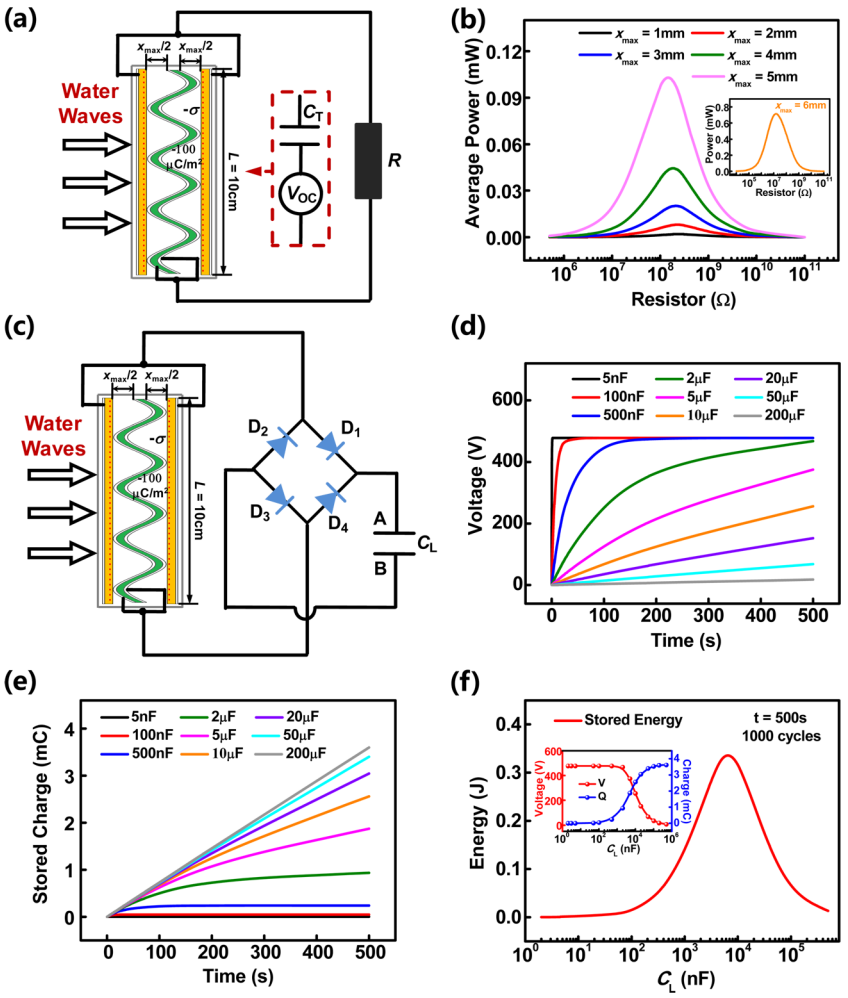

Figure 1. (a) Equivalent circuit model of the wavy-structured TENG connected with a resistor under direct water wave impact. (b) Average output power with respect to the load resistance R for various deformation depths x_{max}. (c) Schematic circuit diagram of the TENG to charge a capacitor through a full-bridge rectifier under direct water wave impact. (d) Voltage−time relationships at different load capacitances C_L when x_{max} = 6 mm. (e) Stored charge−time relationships at different C_L when x_{max} = 6 mm. (f) Influence of load capacitance on the final stored energy, voltage, and charge.

calculated to simulate the direct water wave impact. The influences of load capacitance, charging cycle number, and deformation depth were systematically analyzed in the multicycle charging process. The charging performance of TENG during the enclosed ball collision induced by water waves (in designed sloping collision mode) then was investigated and optimized for various structural parameters, such as the size, mass, or number of enclosed ball. Finally, corresponding experiments were performed to further validate the above theoretical predictions. The combination between theoretical calculations and experimental studies provides the strategies for improving the charging performance of TENGs toward effective water wave energy harvesting and storage.

2. RESULTS AND DISCUSSION

2.1. Charging Characteristic of TENG under Direct Water Wave Impact. The finite element model of a wavy-structured TENG, in which a wavy conductor−dielectric−conductor film was sandwiched between two flat dielectric films, was first constructed as in our previous work.[16] The basic output properties of TENG were simulated by the finite element method (FEM) adopting the same TENG parameters and boundary conditions. Through the continuous fraction interpolation of FEM results, the semianalytical governing equation of TENG was obtained, and then the dynamic output characteristics of TENG at arbitrary load resistance can be numerically calculated by specifying the mechanical motion mode.[26−29] The wavy-structured TENG has been demonstrated to be capable of harvesting the impact energy from water waves.[16,30] Herein, we imposed a periodic triggering at a low frequency on this TENG to simulate the direct water wave impact.

Figure 1a shows the equivalent circuit model of the wavy-structured TENG connected with a resistor under direct water wave impact. The TENG can be modeled as the serial connection of an ideal voltage source (V_{OC}) with a capacitor (C_T).[31] The resistive load performance of TENG under water wave impact was calculated through the following equation:

$$R\frac{dQ}{dt} = V = -\frac{1}{C_T(x)} \times Q + V_{OC}(x) \quad (1)$$

by assigning a harmonic motion mode with the x−t relationship given by

$$x(t) = \frac{x_{max}}{2}(1 - \cos \omega t) \quad (2)$$

DOI: 10.1021/acsami.6b07697
ACS Appl. Mater. Interfaces XXXX, XXX, XXX−XXX

where x_{max} varying from 1 to 6 mm is the compression deformation depth, and angular frequency ω is fixed as 4π (f = 2 Hz). The steady-state output charge, current, and voltage for various resistances were obtained by applying a periodic boundary condition (Figure S1). Note that in the calculations the undeformed state at maximum separation was the initial state, and this state under short-circuit condition was chosen as the charge reference state. The maximum separation was set as 6 mm, so the maximum value of x_{max} is 6 mm. The average output power P_{out} as a function of the resistance for various x_{max} then was captured as shown in Figure 1b. The maximum average power $P_{out,max}$ can be transited at an optimum load resistance for all x_{max} values, and the maximum power increases with increasing x_{max}.

In this work, the charging characteristics of wavy-structured TENG were mainly focused on, and the circuit diagram of the TENG to charge a capacitor through a full-bridge rectifier under direct water wave impact is schematically presented in Figure 1c. The full-bridge diode rectifier can prevent the charge leaking back from load capacitor C_L to the TENG. The nonlinear time-variant system can be simplified to a linear system by neglecting the reverse leakage current of diodes and conducting voltage.[32] In the first half of each charging cycle, the wavy structure is compressed and V_{OC} under the reference state gradually increases. The diodes D_2 and D_4 are conducting, while D_1 and D_3 are fully turned off. A simplified linear circuit without rectifier, in which the serial connection of V_{OC} and C_T is connected with the load capacitor across a node M, can be obtained in Figure S2. In the second half of each charging cycle, the direction of C_L is reversed because of the function of full-bridge rectifier. By utilizing the initial condition that initial charges on both C_T and C_L are zero, we can derive the analytical formulas and calculate the voltage, stored charges, and stored energy on the C_L at the kth charging cycle.

At the beginning of the first charging cycle, the total charges stored on node M are zero ($Q_1^M = 0$, Q_k^M stands for the stored charges on node M at the beginning of the kth charging cycle). During its first half, it is a unidirectional charging process, and voltage $V_{1,1st}^C$ and stored charge $Q_{1,1st}^C$ on C_L can be obtained from the following equations:

$$V_{1,1st}^C = -\frac{1}{C_T(t)} \times Q_{1,1st} + V_{OC}(t) = \frac{Q_{1,1st}^C}{C_L},$$
$$Q_{1,1st}^C = Q_{1,1st} \tag{3}$$

$$V_{1,1st}^C = -\frac{C_T(t)V_{OC}(t)}{C_T(t) + C_L} = \frac{Q_{SC}(t)}{C_T(t) + C_L},$$
$$Q_{1,1st}^C = \frac{C_L Q_{SC}(t)}{C_T(t) + C_L} \tag{4}$$

where $Q_{1,1st}$ is the transferred charge on the inherent capacitor C_T in the first half of the first cycle. For the second half of the first cycle, the direction of C_L is reversed, and the charges stored on node M at the beginning of the second half of the first cycle ($Q_{1,mid}^M$) can be given by

$$Q_{1,mid}^M = -Q_{1,2begin} + Q_{1,2begin}^C = -Q_{1,1end} - Q_{1,1end}^C$$
$$= -\frac{2C_L Q_{SC,max}}{C_{max} + C_L} \tag{5}$$

where $Q_{SC,max}$ and C_{max}, respectively, denote the values of Q_{SC} and C_T at $x = x_{max}$. The voltage $V_{1,2nd}^C$ and stored charge $Q_{1,2nd}^C$ on C_L at the second half of the first cycle then can be calculated by

$$V_{1,2nd}^C = \frac{Q_{SC}(t) + Q_{1,mid}^M}{C_T(t) + C_L},$$
$$Q_{1,2nd}^C = \frac{Q_{SC}(t) + Q_{1,mid}^M}{C_T(t) + C_L} C_L \tag{6}$$

Similarly, the voltage and charge on C_L in the second charging cycle can be calculated (detailed derivations, see Supporting Information, section 2). For clarity, the voltage profiles of V_k^C and $|V_k^C|$ in the first two cycles are shown in Figure S3. Note that the V_k^C exhibits the alternating-current character, because its positive direction is defined from the positive electrode to the negative electrode of TENG, and thus $|V_k^C|$ denotes the real voltage on C_L. Subsequently, for the kth charging cycle, Q_k^M can be obtained by a recursion method:

$$Q_k^M = \frac{C_L - C_{min}}{C_{max} + C_{min}} Q_{SC,max} - \frac{C_L - C_{min}}{C_{max} + C_{min}} Q_{SC,max}$$
$$\times \left[\frac{(C_L - C_{max})(C_L - C_{min})}{(C_L + C_{max})(C_L + C_{min})}\right]^{k-1} \tag{7}$$

The voltage on C_L at the end of kth charging cycle ($|V_{k,2end}^C|$) can be derived as

$$|V_{k,2end}^C| = \frac{Q_{SC,max}}{C_{max} + C_{min}}$$
$$\times \left\{1 - \left[1 - \frac{2(C_{max} + C_{min})C_L}{(C_L + C_{max})(C_L + C_{min})}\right]^k\right\} \tag{8}$$

For a detailed derivation, see Supporting Information, section 2. The stored energy on C_L at the end of kth charging cycle then is calculated by

$$E_{k,end}^C = \frac{C_L(V_{k,2end}^C)^2}{2} = \frac{C_L(Q_{SC,max})^2}{2(C_{max} + C_{min})^2}$$
$$\times \left\{1 - \left[1 - \frac{2(C_{max} + C_{min})C_L}{(C_L + C_{max})(C_L + C_{min})}\right]^k\right\}^2 \tag{9}$$

The charging voltages at different load capacitances C_L when x_{max} = 6 mm are shown in Figure 1d. For all C_L values, the voltage gets the same saturation value gradually similar to a typical resistor−capacitor (RC) charging curve, and the charging speed slows gradually with the evolution of time. The charging speed is larger for smaller C_L, and the time for the voltage to reach saturation is shorter. On the other hand, the stored charges on various C_L when x_{max} = 6 mm were calculated by the product of charging voltage and capacitance C_L as shown in Figure 1e. For smaller C_L values, the stored charge first increases and then gets saturation quickly. As the C_L increases, the stored charge increases, and the curve is elevated until it becomes linear. After 1000 charging cycles, the voltage and stored charge on the load capacitor (inset of Figure 1f) indicate that when C_L is small enough, the voltage on C_L is approximately its saturation voltage while the stored charges are close to zero. In contrast, when C_L is large enough, the

DOI: 10.1021/acsami.6b07697
ACS Appl. Mater. Interfaces XXXX, XXX, XXX−XXX

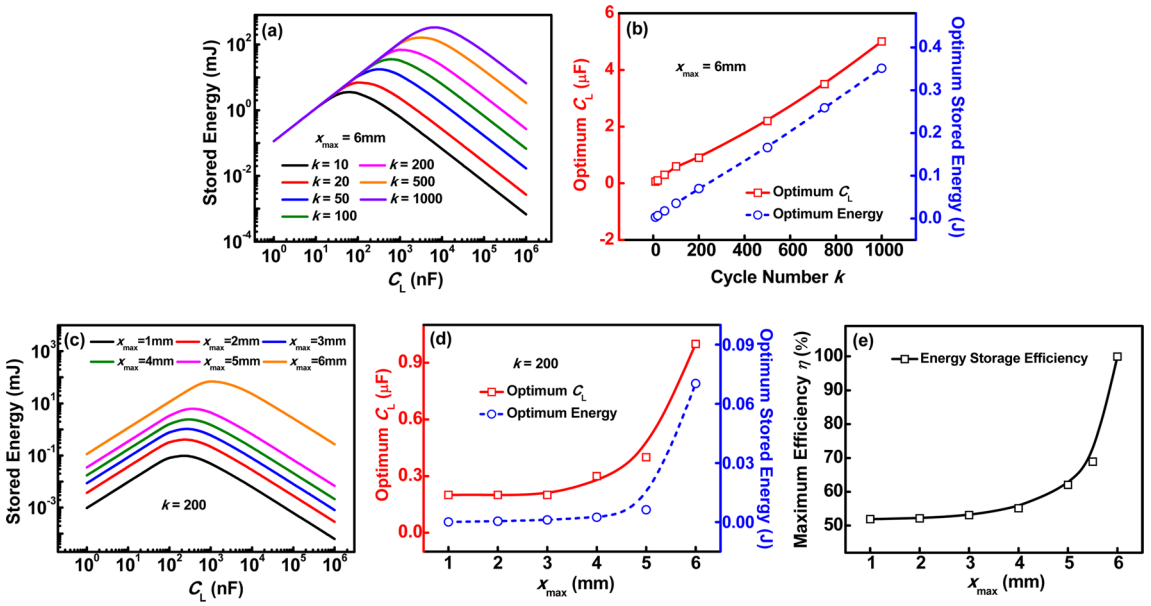

Figure 2. (a) Relationship between stored energy and load capacitance for various cycle numbers k when x_{max} = 6 mm. (b) Extracted optimum capacitance and optimum stored energy for various k. (c) Stored energy with respect to the capacitance C_L under different deformation depths x_{max} at k = 200. (d) Optimum C_L and optimum stored energy as functions of x_{max} at k = 200. (e) Maximum energy storage efficiency for different x_{max}.

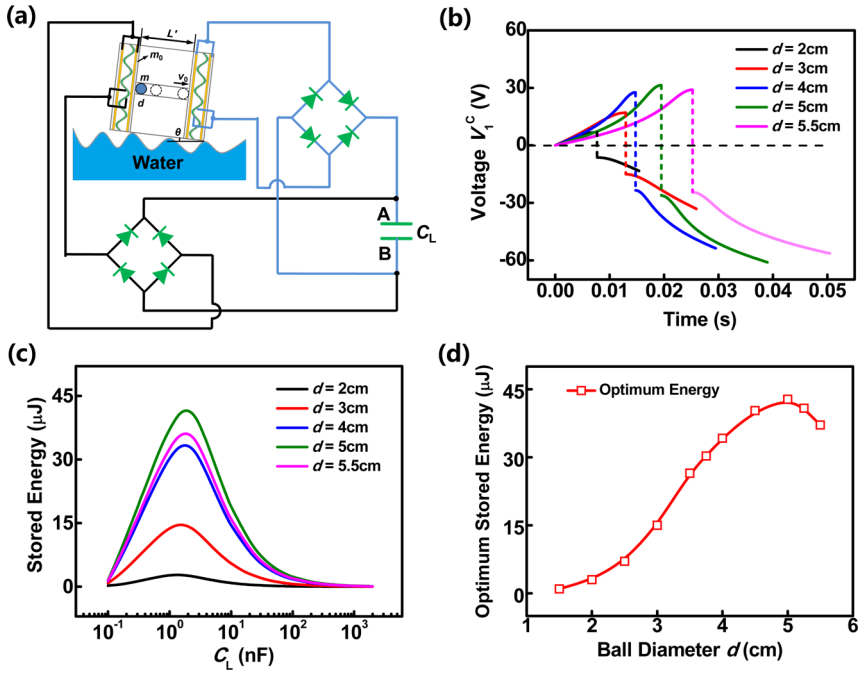

Figure 3. (a) Schematic circuit diagram of the TENG to charge a capacitor through a full-bridge rectifier under the enclosed ball collision. (b) Charging voltage V_1^C on the capacitor (C_L = 10 nF) for various metal ball diameters d in the first charging cycle. The moving length L' and sloping angle θ were set as 6 cm and 30°, respectively. (c) Stored energy with respect to the C_L for various d during the first charging cycle. (d) Optimum stored energy as functions of d during the first charging cycle.

voltage is close to zero and the stored charges are approximately $2kQ_{SC,max}$. These lead to an optimum load capacitance for maximum stored energy after 1000 cycles (Figure 1f).

The stored energies on the capacitor were numerically calculated for various cycle numbers and deformation depths to get further analysis. The relationship between stored energy and C_L for various k when x_{max} = 6 mm is shown in Figure 2a. At smaller C_L, the curves of stored energy coincide for different k because the charging voltage reaches saturation very quickly. There exists an optimum C_L for the stored energy to reach the maximum value for any k, and the maximum stored energy and optimum C_L both increase with increasing k. That can be also viewed from the almost linear relationship between extracted optimum C_L, optimum stored energy, and k in Figure 2b. The stored energy with respect to the capacitance C_L under different deformation depths x_{max} at k = 200 was also examined and shown in Figure 2c. As can be seen, the stored energy increases with the increase of x_{max}, and the optimum C_L shifts toward a larger value due to the increase in the inherent capacitance of

DOI: 10.1021/acsami.6b07697
ACS Appl. Mater. Interfaces XXXX, XXX, XXX−XXX

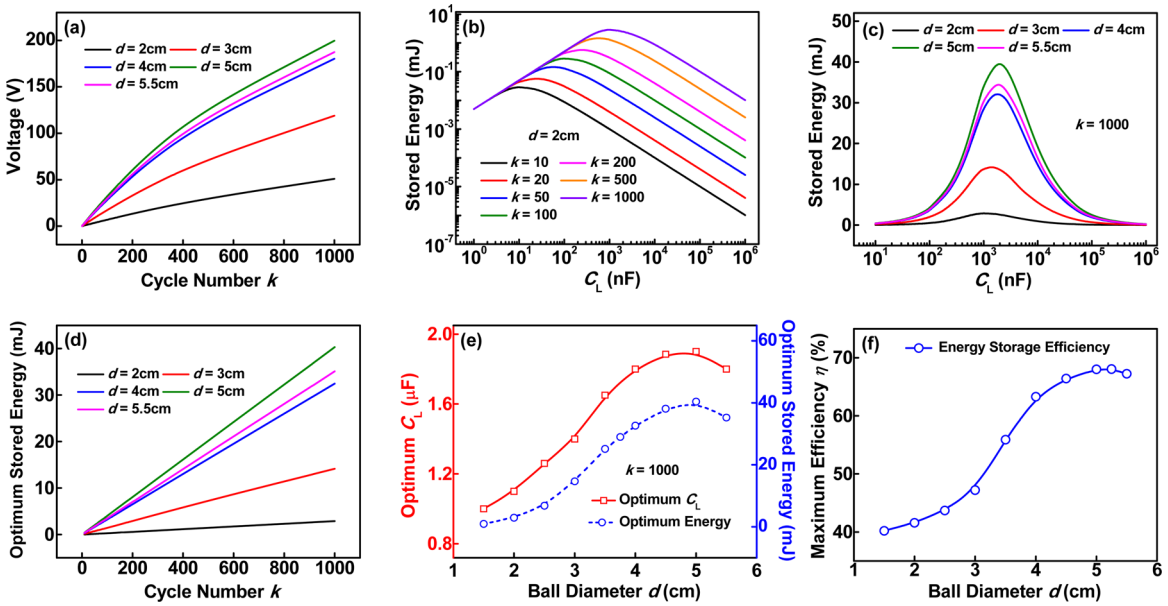

Figure 4. (a) Voltage−cycle number relationship for various ball diameters d at C_L = 2 μF. (b) Relationship between stored energy and load capacitance for different cycle numbers k at d = 2 cm. (c) Stored energy at various load capacitances for various d after 1000 cycles. (d) Optimum stored energy as functions of k for various d. (e) Extracted optimum C_L and optimum stored energy for various d after 1000 cycles. (f) Maximum energy storage efficiency for different d.

TENG. At larger x_{max}, the optimum C_L and optimum stored energy both increase more rapidly (Figure 2d). For the direct water wave impact system, the maximum energy storage efficiency η_{max} is defined by

$$\eta_{max} = \frac{P_{store,max}}{P_{out,max}} \times 100\% = \frac{(E^C_{k,end}/t)_{max}}{P_{out,max}} \times 100\% \quad (10)$$

where the maximum stored power $P_{store,max}$ is the maximum ratio of stored energy to charging time.[33] The maximum efficiency η_{max} was calculated for various x_{max}, as shown in Figure 2e, and it was found to increase with the increase of x_{max}. Note that in this work, we just considered the case of $x_{max} \leq 6$ mm. If the maximum separation is beyond 6 mm (x_{max} is also beyond 6 mm), the efficiency also has the same tendency; that is, it increases with increasing x_{max}. The maximum stored power for a specific x_{max} is independent of the load capacitance C_L, but the charging time to get the maximum stored power is smaller for smaller C_L (Figure S4). The efficiency results reveal that under the direct water wave impact, the stronger impact force reflected by larger x_{max} can enhance the charging performance of wavy-structured TENG.

2.2. Charging Characteristic of TENG under Enclosed Ball Collision. Besides harvesting the impact energies of water waves, we also harvested the wave energies using a full-packaged device floating on water surfaces by means of the collision between an enclosed ball and TENG walls. Triggered by the water wave motion, the sloping of device can induce the occurrence of collision. We designed the sloping collision mode the same as in our previous work to mimic the action of water waves.[16] The sloping angle is defined as θ, and the allowable moving length for the ball is defined as L'. The details can be found in previous work. In this work, we mainly addressed the charging characteristic of the enclosed ball collision system. Figure 3a shows the schematic circuit diagram of the TENG to charge a capacitor through a full-bridge rectifier under the enclosed ball collision. The TENGs anchored onto the internal surface of a sealed box are connected to rectifier bridges and then connected in parallel before charging the capacitor C_L.

We first considered the charging characteristic of TENG for the first charging cycle in designed sloping collision. The charging voltage V_1^C on the capacitor (C_L = 10 nF) for various ball diameters d in the first cycle was calculated on the basis of eqs 4 and 6, and the result is presented in Figure 3b. The two equations in section 2.1 are also suitable for the ball collision system, because the motion mode information was not utilized in our derivation. Without specific notation, the enclosed ball was chosen as a steel ball with a density of 7.9 g/cm^3. V_1^C exhibits the alternating-current character due to the direction transition of C_L at half-cycle. With increasing d, the period of charging cycle increases, and the absolute voltage at the end of the first cycle first increases and then decreases. The total stored energy on C_L during the first cycle then was calculated by the following equation:

$$E^C_{1,end} = \frac{C_L(V^C_{1,2end})^2}{2} = \frac{2C_L{}^3(Q_{SC,max})^2}{(C_L + C_{max})^2(C_L + C_{min})^2} \quad (11)$$

The $E^C_{1,end}$−C_L curves for various d in Figure 3c indicate that there exists an optimum C_L to reach the maximum $E^C_{1,end}$, where the impedance match between the TENG and the load is reached. As for the effect of d, the optimum stored energy was found to increase first and then decrease with increasing d, exhibiting an optimum ball diameter for the ball collision system to get the maximum stored energy on optimum capacitance (Figure 3d).

The charging performance of wavy-structured TENG under the enclosed ball collision was also characterized in a multicycle charging process. The voltage and stored energy on C_L at the end of kth charging cycle were calculated through eqs 8 and 9. The results about the voltage−cycle number relationship for various ball diameters d at C_L = 2 μF are shown in Figure 4a. The voltage profiles have the increasing trend with k similar to

DOI: 10.1021/acsami.6b07697
ACS Appl. Mater. Interfaces XXXX, XXX, XXX−XXX

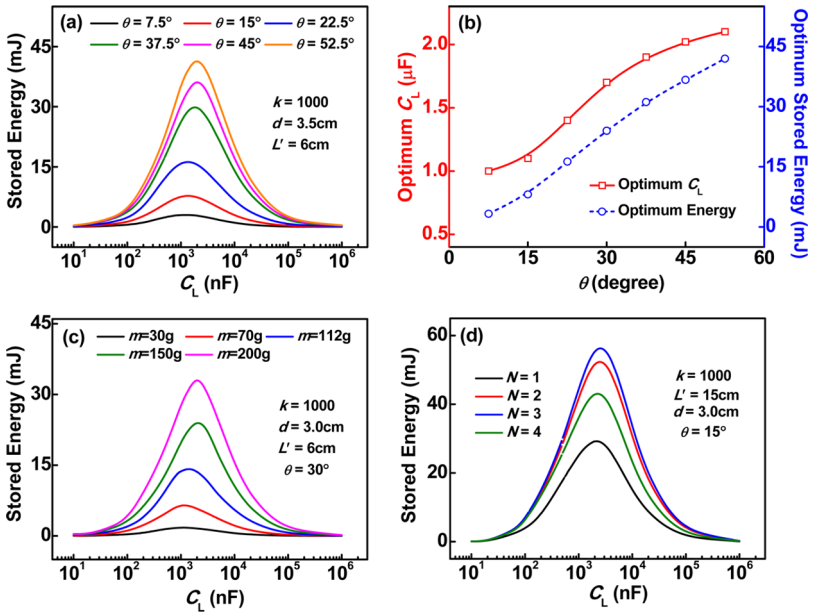

Figure 5. (a) Stored energy at various load capacitances for various sloping angle θ after 1000 cycles at d = 3.5 cm and L' = 6 cm. (b) Influence of θ on the optimum C_L and optimum stored energy after 1000 cycles. (c) Stored energy at various C_L for various ball mass m after 1000 cycles at d = 3.0 cm, L' = 6 cm, and θ = 30°. (d) Stored energy at various C_L for various ball number N after 1000 cycles at L' = 15 cm, d = 3.0 cm, and θ = 15°.

a logarithmic function curve, and as the d increases, the voltage increases first and then decreases with an optimum diameter (d = 5 cm). The relationships between stored energy and load capacitance were investigated for different cycle numbers k and ball diameters d, as shown in Figure 4b,c. An optimum C_L was observed for the system to reach the maximum stored energy for any k and d. When k increases (d = 2 cm), the optimum stored energy increases and the optimum C_L shifts right to a larger value. The increase of optimum stored energy with k is linear for various d (Figure 4d), which is the same as the case of direct water wave impact. When we changed the ball diameter d, the optimum stored energy after 1000 cycles possesses a maximum value at the optimum diameter of d = 5 cm (Figure 4c). Similar to the optimum stored energy, for the optimum C_L, there is also an optimum diameter as shown in Figure 4e. The existing optimum ball diameter for charging performance can be ascribed to competition between ball mass and allowable moving space, similar to the output performance.[16]

To demonstrate the linear relationship between optimum stored energy $E^C_{k,\mathrm{end,opt}}$ (or optimum load capacitance $C_{L,\mathrm{opt}}$) and k, we provided an approximate analytical solution to $E^C_{k,\mathrm{end,opt}}$ and $C_{L,\mathrm{opt}}$. Usually, the C_L is much larger than both $C_{\max}$ and $C_{\min}$, and eq 8 can be simplified as

$$|V^C_{k,2\mathrm{end}}| = \frac{Q_{SC,\max}}{C_{\max}+C_{\min}}\left\{1-\exp\left[-\frac{2(C_{\max}+C_{\min})k}{C_L}\right]\right\} \quad (12)$$

Equation 9 can be changed into

$$E^C_{k,\mathrm{end}} = \frac{C_L(Q_{SC,\max})^2}{2(C_{\max}+C_{\min})^2} \times \left\{1-\exp\left[-\frac{2(C_{\max}+C_{\min})k}{C_L}\right]\right\}^2 \quad (13)$$

On the basis of the zero differentiation of $E^C_{k,\mathrm{end}}$ by C_L at $C_{L,\mathrm{opt}}$, we can obtain the analytical solutions:

$$C_{L,\mathrm{opt}} = 1.5918k(C_{\max}+C_{\min}) \quad (14)$$

$$E^C_{k,\mathrm{end,opt}} = \frac{0.4073k(Q_{SC,\max})^2}{C_{\max}+C_{\min}} \quad (15)$$

The two equations are excellent estimations at larger k (>10) and also applicable to other categories of TENGs.

In addition, the stored power P_{store} can be derived from eq 13:

$$P_{\mathrm{store}} = \frac{E^C_{k,\mathrm{end}}}{t} = \frac{f(Q_{SC,\max})^2}{C_{\max}+C_{\min}} \times \frac{\{1-\exp[-2(C_{\max}+C_{\min})ft/C_L]\}^2}{2(C_{\max}+C_{\min})ft/C_L} \quad (16)$$

where f stands for the frequency of periodic motion, and at the optimized charging time $t_{\mathrm{opt}} = 0.6282C_L/f(C_{\max}+C_{\min})$, P_{store} reaches its maximum value:

$$P_{\mathrm{store,max}} = \frac{0.4073f(Q_{SC,\max})^2}{C_{\max}+C_{\min}} \quad (17)$$

This equation can also verify that the maximum stored power is independent of C_L as shown in Figure S4. The maximum energy storage efficiency under the enclosed ball collision then can be given by

$$\eta_{\max} = \frac{P_{\mathrm{store,max}}}{P_{\mathrm{out,max}}} \times 100\% = \frac{0.4073(Q_{SC,\max})^2}{(C_{\max}+C_{\min})(E_{\mathrm{out,per}})_{\max}} \times 100\% \quad (18)$$

where $(E_{\mathrm{out,per}})_{\max}$ is the maximum output energy per cycle. The maximum efficiency $\eta_{\max}$ was calculated for different d, and it can be found from Figure 4f that an optimum d also exists for the ball collision system to reach the maximum of $\eta_{\max}$. Note

DOI: 10.1021/acsami.6b07697
ACS Appl. Mater. Interfaces XXXX, XXX, XXX−XXX

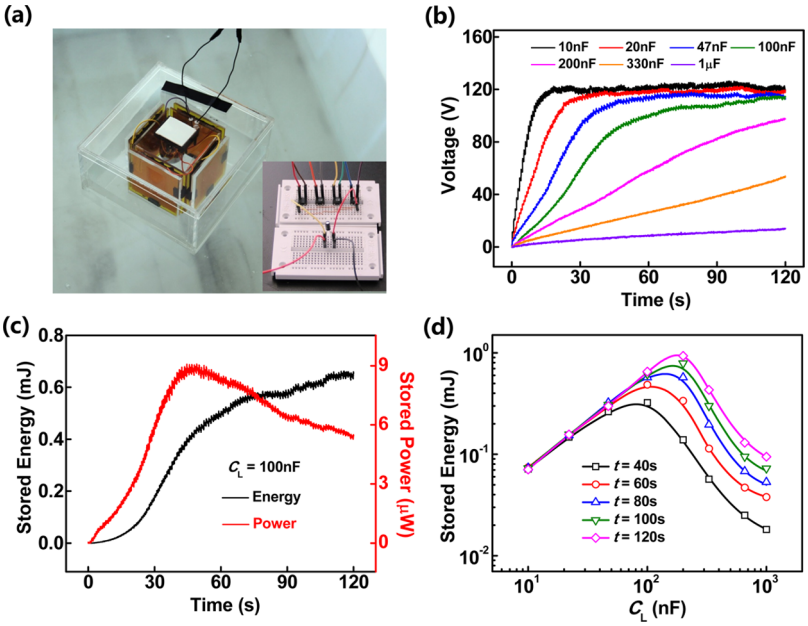

Figure 6. (a) Photograph of a sealed TENG device floating on water in a pool. The inset shows a schematic photo of the connection fashion between TENGs and the load capacitor through the bridge rectifiers. (b) Charging voltage on various load capacitances C_L under the enclosed ball collision. (c) Stored energy−time relationship and stored power−time relationship for a fixed capacitor (C_L = 100 nF). (d) Stored energy with respect to the load capacitance for various charging time.

that the calculation methods of stored energy and maximum efficiency are also applicable to TENGs with other structures for harvesting water wave energy. Some conclusions are also suitable for all TENG structures, because we did not utilize any TENG category information in our formula derivations. For example, the stored energy reaches its peak value at an optimum load capacitance, and both the optimum stored energy and the optimum C_L increase with increasing k. However, for different TENG structures, the influences of different structural parameters on the stored energy or efficiency may be different.

In addition to the influence of ball diameter, we also studied the influences of sloping angle θ, ball mass m, and ball number N on the charging characteristics of the TENG during its collision with an enclosed ball. The sloping angle-dependent charging behavior for d = 3.5 cm and L' = 6 cm is shown in Figure 5a,b. The optimum stored energy after 1000 cycles was found to increase with increasing sloping angle, implying that the larger is the wave height, the higher is the storage. Also, the optimum C_L has a little increase with the increase of θ (Figure 5b). In the above calculations, the ball was chosen as a steel ball with a constant ratio of ball mass to ball volume. If the ball is hollow with variable void ratios or it has different materials, the ball mass m is variable for a fixed ball size. Figure 5c presents the stored energy with respect to C_L for various ball masses after 1000 cycles at d = 3.0 cm, L' = 6 cm, and θ = 30°. The results indicate that the optimum stored energy increases with increasing the mass, which is similar to the output characteristic. The increase in ball mass results in a faster compression and a larger deformation depth at a constant allowable moving space. For the effect of ball number, with the assumption that the metal balls move synchronously in a specific orbit with their mutual collision or separation prevented, the stored energy−C_L curves after 1000 cycles were plotted in Figure 5d for various N at L' = 15 cm, d = 3.0 cm, and θ = 15°. The optimum stored energy has the maximum for three balls.

To verify the above theoretical predictions on the charging characteristics of TENG under enclosed ball collision, we carried out the corresponding experiments of real water wave tests. The wavy-structured TENGs with a wavy Cu−Kapton−Cu film sandwiched between two fluorinated ethylene propylene (FEP) thin films coated by Cu were utilized in the experiments. Four such TENGs were anchored as standing walls, allowing a metal ball to form the single unit of TENG network. The experimental details can be found in Supporting Information, section 3. Figure 6a shows a photo of a sealed device floating on water in a pool and a schematic photo of the connection fashion between TENGs and the load capacitor through the bridge rectifiers. Four TENGs are respectively connected to a full-bridge rectifier and then connected in parallel. We used the sealed device to charge various capacitors by adopting a single and constant wave condition. In the experimental measurements, the water waves were generated through the seesawing motion of tank with water inside at fixed amplitude and frequency.

The charging voltage on various load capacitances C_L under the enclosed ball collision was measured by a voltage meter (Keithley 6514 System electrometer), as shown in Figure 6b. The trends of charging voltage with the charging time and C_L are in accordance with the theoretical results shown in Figure 1d. At zero time, the capacitor is charged at the maximum speed, and then the charging speed slows gradually until 0. The voltage for all capacitances finally reaches the same saturation voltage, and it takes less time to charge a smaller C_L to reach the saturation voltage. The stored energy−time relationship and stored power−time relationship for a fixed capacitor (C_L = 100 nF) were plotted in Figure 6c. From that, we can see that the stored energy increases to saturation gradually, and there exists the optimum charging time to get the maximum stored power. The optimum charging time can correspond to an optimum charging voltage, and the maximum storage efficiency. The curves of the stored energy with respect to the load

DOI: 10.1021/acsami.6b07697
ACS Appl. Mater. Interfaces XXXX, XXX, XXX−XXX

capacitance for various charging time presented in Figure 6d indicate the maximized stored energy can be observed at optimum C_L. The increases of optimum stored energy and optimum C_L with the charging time are in good agreement with the theoretical results (Figure 4b). The above experimental results can further validate our theoretical predictions, and, conversely, the theoretical results can guide future experimental designs. This work provides the optimization approach of charging performances of wavy-structured TENG, which will facilitate the applications of TENG technology on the blue energy harvesting.

Finally, we need to emphasize the relationship and differences between this work and the previous work. This work is a subsequent study of the previous work,[16] but they are also different. In the previous work, the output performance of triboelectric nanogenerator, for example, output power and electric energy, was mainly investigated and optimized from the viewpoint of TENG structure. However, in this work, we mainly addressed the charging characteristics of TENG to a capacitor, including the stored energy and stored efficiency associated with the structural parameters or load capacitance. Understanding the integration behavior of TENG with an energy storage unit and further optimizing the charging system can provide useful guidance for efficient water wave energy harvesting and storage.

3. CONCLUSIONS

In summary, we have optimized the charging performance of a wavy-structured TENG to a capacitor in two cases, that is, under the direct water wave impact and enclosed ball collision. On the basis of the FEM simulations and analytical equation derivations, the charging characteristics of TENG when imposed as a periodic triggering at a low frequency and when colliding with a metal ball in designed sloping collision were theoretically calculated. The results indicate that the stored energy can reach the maximum value at an optimum load capacitance for all situations. The stored energy−capacitance relationship and maximum energy storage efficiency under the direct water wave impact are greatly affected by the compression deformation depth. On the other hand, there exists an optimum ball diameter, mass, or number for the enclosed ball collision system to reach maximized stored energy and efficiency. The real water wave measurements then also present the same charging behavior as the theoretical predictions. This work could provide useful information for charging performance optimization of TENGs for effective water wave energy harvesting and storage toward large-scale blue energy harvesting.

■ ASSOCIATED CONTENT

Supporting Information

The Supporting Information is available free of charge on the ACS Publications website at DOI: 10.1021/acsami.6b07697.

Dynamic output characteristic of TENG under direct water wave impact, formula derivations, and calculation results on charging characteristic of TENG under direct water wave impact, and the experimental details (PDF)

■ AUTHOR INFORMATION

Corresponding Author

*E-mail: zlwang@gatech.edu.

Author Contributions

[§]Y.Y. and T.J. contributed equally.

Notes

The authors declare no competing financial interest.

■ ACKNOWLEDGMENTS

Support from the "thousands talents" program for the pioneer researcher and his innovation team, China, the National Natural Science Foundation of China (Grant nos. 51432005, 5151101243, 51561145021, and 61405131), and the Project funded by the China Postdoctoral Science Foundation (2016M590070) is appreciated.

■ REFERENCES

(1) Khaligh, A.; Onar, O. C. *Energy Harvesting: Solar, Wind, and Ocean Energy Conversion Systems*; CRC Press: Boca Raton, FL, 2009.
(2) Painuly, J. P. Barriers to Renewable Energy Penetration: A Framework for Analysis. *Renewable Energy* **2001**, *24*, 73−89.
(3) Boyle, G. *Renewable Energy: Power for a Sustainable Future*; Oxford University Press: Oxford, UK, 1996.
(4) Salter, S. H. Wave Power. *Nature* **1974**, *249*, 720−724.
(5) Falnes, J. A Review of Wave-Energy Extraction. *Mar. Struct.* **2007**, *20*, 185−201.
(6) Jouanne, A. V. Harvesting the Waves. *Mech. Eng. Mag.* **2006**, *128*, 24−27.
(7) Henderson, R. Design, Simulation, and Testing of a Novel Hydraulic Power Take-Off System for the Pelamis Wave Energy Converter. *Renewable Energy* **2006**, *31*, 271−283.
(8) Wolfbrandt, A. Automated Design of a Linear Generator for Wave Energy Converters-A Simplified Model. *IEEE Trans. Magn.* **2006**, *42*, 1812−1819.
(9) Fan, F. R.; Tian, Z. Q.; Wang, Z. L. Flexible Triboelectric Generator. *Nano Energy* **2012**, *1*, 328−334.
(10) Tang, W.; Jiang, T.; Fan, F. R.; Yu, A. F.; Zhang, C.; Cao, X.; Wang, Z. L. Liquid-Metal Electrode for High-Performance Triboelectric Nanogenerator at an Instantaneous Energy Conversion Efficiency of 70.6%. *Adv. Funct. Mater.* **2015**, *25*, 3718−3725.
(11) Zhu, G.; Zhou, Y. S.; Bai, P.; Meng, X. S.; Jing, Q.; Chen, J.; Wang, Z. L. A Shape-Adaptive Thin-Film-Based Approach for 50% High-Efficiency Energy Generation through Micro-Grating Sliding Electrification. *Adv. Mater.* **2014**, *26*, 3788−3796.
(12) Wang, S. H.; Lin, L.; Wang, Z. L. Triboelectric Nanogenerators as Self-Powered Active Sensors. *Nano Energy* **2015**, *11*, 436−462.
(13) Xie, Y. N.; Wang, S. H.; Niu, S. M.; Lin, L.; Jing, Q. S.; Yang, J.; Wu, Z. Y.; Wang, Z. L. Grating-Structured Freestanding Triboelectric-Layer Nanogenerator for Harvesting Mechanical Energy at 85% Total Conversion Efficiency. *Adv. Mater.* **2014**, *26*, 6599−6607.
(14) Wang, Z. L. Triboelectric Nanogenerators as New Energy Technology and Self-Powered Sensors − Principles, Problems and Perspectives. *Faraday Discuss.* **2014**, *176*, 447−488.
(15) Chen, J.; Yang, J.; Li, Z. L.; Fan, X.; Zi, Y. L.; Jing, Q. S.; Guo, H. Y.; Wen, Z.; Pradel, K. C.; Niu, S. M.; Wang, Z. L. Networks of Triboelectric Nanogenerators for Harvesting Water Wave Energy: A Potential Approach toward Blue Energy. *ACS Nano* **2015**, *9*, 3324−3331.
(16) Jiang, T.; Zhang, L. M.; Chen, X. Y.; Han, C. B.; Tang, W.; Zhang, C.; Xu, L.; Wang, Z. L. Structural Optimization of Triboelectric Nanogenerator for Harvesting Water Wave Energy. *ACS Nano* **2015**, *9*, 12562−12572.
(17) Wang, X. F.; Niu, S. M.; Yin, Y. J.; Yi, F.; You, Z.; Wang, Z. L. Triboelectric Nanogenerator Based on Fully Enclosed Roolling Spherical Structure for Harvesting Low-Frequency Water Wave Energy. *Adv. Energy Mater.* **2015**, *5*, 1501467.
(18) Zhu, G.; Su, Y. J.; Bai, P.; Chen, J.; Jing, Q. S.; Yang, W. Q.; Wang, Z. L. Harvesting Water Wave Energy by Asymmetric Screening of Electrostatic Charges on a Nanostructured Hydrophobic Thin-Film Surface. *ACS Nano* **2014**, *8*, 6031−6037.

DOI: 10.1021/acsami.6b07697
ACS Appl. Mater. Interfaces XXXX, XXX, XXX−XXX

(19) Lin, Z.-H.; Cheng, G.; Lin, L.; Lee, S.; Wang, Z. L. Water-Solid Surface Contact Electrification and its Use for Harvesting Liquid Wave Energy. *Angew. Chem., Int. Ed.* **2013**, *52*, 12545−12549.
(20) Zhang, L.; Han, C. B.; Jiang, T.; Zhou, T.; Li, X.; Zhang, C.; Wang, Z. L. Multilayer Wavy-Structured Robust Triboelectric Nanogenerator for Harvesting Water Wave Energy. *Nano Energy* **2016**, *22*, 87−94.
(21) Liang, Q.; Yan, X.; Liao, X.; Cao, S.; Zheng, X.; Si, H.; Lu, S.; Zhang, Y. Multi-Unit Hydroelectric Generator Based on Contact Electrification and Its Service Behavior. *Nano Energy* **2015**, *16*, 329−338.
(22) Liang, Q.; Yan, X.; Gu, Y.; Zhang, K.; Liang, M.; Lu, S.; Zheng, X.; Zhang, Y. Highly Transparent Triboelectric Nanogenerator for Harvesting Water-Related Energy Reinforced by Antireflection Coating. *Sci. Rep.* **2015**, *5*, 9080.
(23) Liang, Q.; Yan, X.; Liao, X.; Zhang, Y. Integrated Multi-Unit Transparent Triboelectric Nanogenerator Harvesting Rain Power for Driving Electronics. *Nano Energy* **2016**, *25*, 18−25.
(24) Pu, X.; Liu, M. M.; Li, L. X.; Zhang, C.; Pang, Y. K.; Jiang, C. Y.; Shao, L. H.; Hu, W. G.; Wang, Z. L. Efficient Charging of Li-Ion Batteries with Pulsed Output Current of Triboelectric Nanogenerators. *Adv. Sci.* **2016**, *3*, 1500255.
(25) Zi, Y. L.; Wang, J.; Wang, S. H.; Li, S. M.; Wen, Z.; Guo, H. Y.; Wang, Z. L. Effective Energy Storage from a Triboelectric Nanogenerator. *Nat. Commun.* **2016**, *7*, 10987−10998.
(26) Niu, S. M.; Liu, Y.; Wang, S. H.; Lin, L.; Zhou, Y. S.; Hu, Y. F.; Wang, Z. L. Theory of Sliding-Mode Triboelectric Nanogenerators. *Adv. Mater.* **2013**, *25*, 6184−6193.
(27) Niu, S. M.; Liu, Y.; Wang, S. H.; Lin, L.; Zhou, Y. S.; Hu, Y. F.; Wang, Z. L. Theoretical Investigation and Structural Optimization of Single-Electrode Triboelectric Nanogenerators. *Adv. Funct. Mater.* **2014**, *24*, 3332−3340.
(28) Jiang, T.; Tang, W.; Chen, X.; Han, C. B.; Lin, L.; Zi, Y.; Wang, Z. L. Figure-of-Merits for Rolling-Friction-Based Triboelectric Nanogenerators. *Adv. Mater. Technol.* **2016**, *1*, 1600017.
(29) Jiang, T.; Chen, X.; Yang, K.; Han, C. B.; Tang, W.; Wang, Z. L. Theoretical Study on Rotary-Sliding Disk Triboelectric Nanogenerators in Contact and Non-Contact Modes. *Nano Res.* **2016**, *9*, 1057−1070.
(30) Wen, X. N.; Yang, W. Q.; Jing, Q. S.; Wang, Z. L. Harvesting Broadband Kinetic Impact Energy from Mechanical Triggering/Vibration and Water Waves. *ACS Nano* **2014**, *8*, 7405−7412.
(31) Niu, S. M.; Wang, Z. L. Theoretical Systems of Triboelectric Nanogenerators. *Nano Energy* **2015**, *14*, 161−192.
(32) Niu, S. M.; Liu, Y.; Zhou, Y. S.; Wang, S. H.; Lin, L.; Wang, Z. L. Optimization of Triboelectric Nanogenerator Charging Systems for Efficient Energy Harvesting and Storage. *IEEE Trans. Electron Devices* **2015**, *62*, 641−648.
(33) Niu, S. M.; Wang, X. F.; Yi, F.; Zhou, Y. S.; Wang, Z. L. A Universal Self-Charging System Driven by Random Biomechanical Energy for Sustainable Operation of Mobile Electronics. *Nat. Commun.* **2015**, *6*, 8975−8986.

DOI: 10.1021/acsami.6b07697
ACS Appl. Mater. Interfaces XXXX, XXX, XXX−XXX